

Two nearby states in the $X(3872)$ region: Resolving the radiative-decay ratio tension with η_{c2}

Satoshi X. Nakamura^{1,*}

¹*Institute of Frontier and Interdisciplinary Science,
Shandong University, Qingdao, Shandong 266237, China*

Recently, LHCb reported the radiative-decay ratio $\mathcal{R}^{\psi\gamma} \equiv \mathcal{B}[X(3872) \rightarrow \psi'\gamma]/\mathcal{B}[X(3872) \rightarrow J/\psi\gamma] = 1.67 \pm 0.25$ extracted from $B^+ \rightarrow K^+(J/\psi\gamma, \psi'\gamma)$. This result differs markedly ($\sim 4.6\sigma$) from the BESIII value obtained from $e^+e^- \rightarrow \gamma(J/\psi\gamma, \psi'\gamma)$, $\mathcal{R}^{\psi\gamma} = -0.04 \pm 0.28$. Such a significant tension suggests that more than one state in the $X(3872)$ region contributes to the processes. We therefore propose a two-state scenario: a shallow $D^{*0}\bar{D}^0$ bound state with $J^{PC} = 1^{++}$ and a 2^{-+} charmonium candidate, η_{c2} , slightly above the $D^{*0}\bar{D}^0$ threshold. We show that this hypothesis consistently describes these ratios along with other branching fractions and lineshapes across multiple processes. By contrast, fits without the η_{c2} component fail to reproduce the radiative-ratio data. We also predict helicity-angle distributions that motivates the future experiments to test the two-state hypothesis and search for the so-far missing η_{c2} .

Introduction.— The 2003 discovery of $X(3872)$ [1] ignited a modern era of hadron spectroscopy [2–10] by highlighting limitations of the traditional quark model [11, 12].¹ Lying essentially at the $D^{*0}\bar{D}^0$ threshold, $X(3872)$ exhibits a dual character: its mass and the narrow width favor a loosely bound hadronic molecule [14–17], while its prompt production rates point to a more compact component [18–24]. Lattice QCD also found an s -wave $D^{*0}\bar{D}^0$ bound state consistent with $X(3872)$ [25, 26].

Here we point out that existing data actually strain the assumption that a single state dominates the $X(3872)$ region. To quantify this, we define the ratio

$$\mathcal{R}_B(f, f') = \frac{\Gamma[B^+ \rightarrow K^+ X(3872); X(3872) \rightarrow f]}{\Gamma[B^+ \rightarrow K^+ X(3872); X(3872) \rightarrow f']}, \quad (1)$$

with $f^{(\prime)} = J/\psi\pi^+\pi^-, J/\psi\omega, D^{*0}\bar{D}^0 + c.c., J/\psi\gamma$, and $\psi'\gamma$; $\Gamma[B^+ \rightarrow K^+ X; X \rightarrow f^{(\prime)}]$ is an $X(3872)$ contribution to a $B^+ \rightarrow K^+ f^{(\prime)}$ partial decay width, obtained through experimental analysis. Similarly, $\mathcal{R}_{e^+e^-}$ is defined by replacements $\Gamma \rightarrow \sigma$ (cross section), $B^+ \rightarrow e^+e^-$ and $K^+ \rightarrow \gamma$ in Eq. (1).

We expect $\mathcal{R}_B(f, f') \sim \mathcal{R}_{e^+e^-}(f, f') \sim \mathcal{B}[X(3872) \rightarrow f]/\mathcal{B}[X(3872) \rightarrow f']$, assuming that the experimental $\Gamma[B^+ \rightarrow K^+ X; X \rightarrow f^{(\prime)}]$ contain sufficiently isolated $X(3872)$ contributions. However, previous experiments found $\mathcal{R}_B(J/\psi\gamma, J/\psi\pi^+\pi^-) = 0.22 \pm 0.07^2$ [27, 28] and $\mathcal{R}_{e^+e^-}(J/\psi\gamma, J/\psi\pi^+\pi^-) = 0.79 \pm 0.28$ [29], giving a difference of $\sim 2\sigma$. Even more strikingly, $\mathcal{R}_x^{\psi\gamma} \equiv \mathcal{R}_x(\psi'\gamma, J/\psi\gamma)$ with $x = B$ or e^+e^- were reported to be

$\mathcal{R}_B^{\psi\gamma} = 1.67 \pm 0.25$ [30] and $\mathcal{R}_{e^+e^-}^{\psi\gamma} = -0.04 \pm 0.28$ [29], giving a difference of $\sim 4.6\sigma$.

Reconciling these results with a single $X(3872)$ state would require an unexpectedly strong process dependence of $\mathcal{R}_x^{\psi\gamma}$, for example from residual backgrounds, fit-model assumptions, or underestimated systematic uncertainties. Rather, the puzzling $\mathcal{R}_x^{\psi\gamma}$ can be naturally understood by considering two distinct states X_A and X_B , and supposing that: (i) $\psi'\gamma$ ($J/\psi\gamma$) events arise predominantly from X_A (X_B) decays; (ii) the production of X_A relative to X_B is substantially enhanced in B^+ decays compared with e^+e^- annihilations.

We next identify the two inferred contributions. From analyses of $B^+ \rightarrow K^+(J/\psi\pi^+\pi^-)$, the $X(3872)$ properties are well constrained, with $m_{X(3872)} = 3871.64 \pm 0.06$ MeV [28]³ and $J^{PC} = 1^{++}$ [31]. It is therefore natural to identify X_A with the established $X(3872)$, interpreted as a shallow $D^{*0}\bar{D}^0$ bound state (with a small $c\bar{c}$ admixture) that accounts for the observed isospin-violating decay strength [32, 33] and accommodates a wide range of relative branching ratios to $\psi'\gamma$ and $J/\psi\gamma$ [34–37].

Regarding X_B , previous analyses hinted at a nearby 2^{-+} charmonium (η_{c2}) decaying into $J/\psi\omega$ [38] and $D^{*0}\bar{D}^0$ [39]. An η_{c2} in this mass region is also expected in quark models [11, 12, 40] and lattice QCD [41, 42], but has not yet been observed [43, 44]. Moreover, its radiative decay is expected to favor $J/\psi\gamma$ over $\psi'\gamma$ [45–47]. We therefore identify X_B with an η_{c2} lying slightly above the $D^{*0}\bar{D}^0$ threshold. An isospin-violating η_{c2} decay, expected to be small, would not affect the J^{PC} determination using the $J/\psi\pi^+\pi^-$ data [31]. This two-state picture

¹ We follow the particle naming convention of the Particle Data Group (PDG) [13]. We also denote $\psi(2S)$, $\psi(4230)$, and $\chi_{c1}(3872)$ by ψ' , $Y(4230)$, and $X(3872)$, respectively. The notation $\{D^*\bar{D}\}$ indicates the positive C -parity state such as $(D^{*0}\bar{D}^0 + \bar{D}^{*0}D^0)/\sqrt{2}$ in our convention.

² Statistical and systematic uncertainties are summed in quadrature throughout this paper.

³ We denote a particle x 's mass, momentum, energy, width, and spin state in the total center-of-mass (CM) frame by m_x , \mathbf{p}_x , E_x , Γ_x , and s_x^z , respectively; $E_x = \sqrt{m_x^2 + \mathbf{p}_x^2}$ with $p_x^2 = |\mathbf{p}_x|^2$. The mass and width values are from the PDG [13]. See the Supplemental Material for the energy dependence of Γ_x .

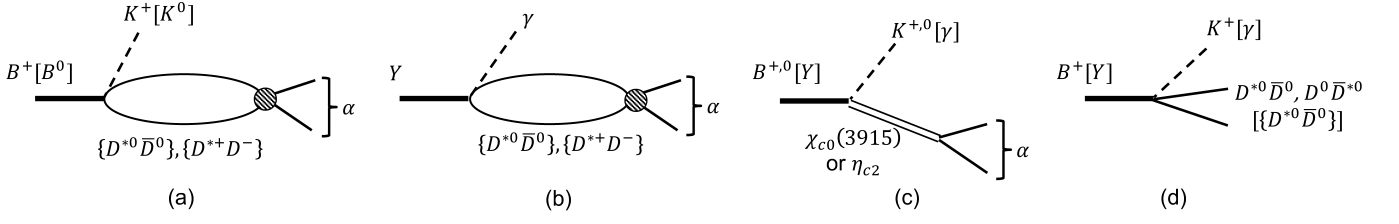


FIG. 1. $B^{+,0}$ and $Y(4230)$ decay mechanisms. Final states α include $J/\psi\rho$, $J/\psi\omega$, $\{D^{*0}\bar{D}^0\}$, $J/\psi\gamma$, and $\psi'\gamma$. The shaded blobs are the rescattering amplitude that generates the $X(3872)$ pole.

also explains why the mass extracted from $J/\psi\omega$ [38, 48] and $D^{*0}\bar{D}^0$ [39, 61] data tends to be 2–3 MeV higher than that from $J/\psi\pi^+\pi^-$ [28, 49]. Although several issues in assigning 2^{-+} to $X(3872)$ have been critically examined [50–52], most of them do not apply to the two-state hypothesis.

In this work, we develop a two-state model that consistently describes a broad set of $X(3872)$ data and highlights clear advantages over a single-state description. We also predict helicity-angle distributions with which the future experiments can test the two-state hypothesis and search for the missing η_{c2} .

Method.— We analyze $B^{+(0)} \rightarrow K^{+(0)}f$ and $e^+e^- \rightarrow \gamma f$ data using the decay mechanisms summarized in Fig. 1. For $e^+e^- \rightarrow \gamma f$, we work at $\sqrt{s} = m_{Y(4230)}$ and model the production as $e^+e^- \rightarrow Y(4230) \rightarrow \gamma f$, following Refs. [17, 48]. In Figs. 1(a,b), $X(3872)$ emerges as a pole of a $J^{PC} = 1^{++}$ coupled-channel system dominated by the $\{D^*\bar{D}\}$ channels. Any compact $c\bar{c}$ component [53, 54] is treated effectively through short-range contact interactions. We additionally include an explicit η_{c2} -excitation mechanism [Fig. 1(c)] to address the radiative-ratio tension. To describe peaks at $M_{J/\psi\omega} \sim 3.92$ GeV [38, 48], we follow the BABAR analysis [55] and include the $\chi_{c0}(3915)$ -excitation mechanism [Fig. 1(c)]. An alternative 2^+ state [56] would not significantly change our result since 1^+ $X(3872)$ interferes with neither 0^+ nor 2^+ states in the $M_{J/\psi\omega}$ distribution.

For the $X(3872)$ production mechanism in B -decay [Fig. 1(a)], the initial weak vertex $B \rightarrow D^*\bar{D}K$ is parameterized as

$$v_{D^*\bar{D}K}^B = c_{D^*\bar{D}K}^B f_{D^*\bar{D}}^0 F_{KB}^1 \mathbf{p}_K \cdot \boldsymbol{\epsilon}_{D^*}, \quad (2)$$

$$A_{B^+ \rightarrow K^+ \alpha}^{(\alpha)} = \mathbf{p}_{K^+} \cdot \boldsymbol{\epsilon}_\alpha \sum_{\beta'} f_\alpha^0(q_\alpha, \Lambda_v) G_{\alpha, \beta'}(p_{K^+}, E) \frac{h_{\beta', \alpha}}{\sqrt{2}} \left(\sum_x^{D^*\bar{D}, D\bar{D}^*} c_{xK^+}^{B^+} \sigma_\beta^{\Lambda_v \Lambda_B}(p_{K^+}, E) \right) F_{K^+ B^+}^1(p_{K^+}, \Lambda), \quad (5)$$

with $E = m_{B^+} - E_{K^+}$; $\beta = \{D^{*0}\bar{D}^0\}$ for $x = D^{*0}\bar{D}^0, D^0\bar{D}^{*0}$ and $\beta = \{D^{*+}D^-\}$ for $x = D^{*+}\bar{D}^-, D^-\bar{D}^{*+}$; $\boldsymbol{\epsilon}_\alpha$ is the total spin polarization of α .

with coupling constant $c_{D^*\bar{D}K}^B$. The $B \rightarrow D\bar{D}^*K$ vertex with $c_{D\bar{D}^*K}^B$ is similar. The B^+ decays include color-favored couplings [57] $c_{D^{*0}\bar{D}^0K^+}^{B^+} \neq c_{D^0\bar{D}^{*0}K^+}^{B^+}$ and color-suppressed couplings $c_{D^{*+}D^-K^+}^{B^+} = c_{D^+D^*K^+}^{B^+}$. Regarding the weak B^0 -decay couplings, we use relations: $c_{D^{*+}D^-K^0}^{B^0} = c_{D^{*0}\bar{D}^0K^+}^{B^0}$, $c_{D^+D^*K^0}^{B^0} = c_{D^0\bar{D}^{*0}K^+}^{B^0}$, and $c_{D^{*0}\bar{D}^0K^0}^{B^0} = c_{D^{*+}D^-K^+}^{B^0}$. The vertices in Eq. (2) include dipole form factors, $f_{ij}^L(q_{ij}, \Lambda_B)$ and $F_{kl}^{L'}(p_k, \Lambda)$,

$$f_{ij}^L = \frac{(1 + q_{ij}^2/\Lambda_B^2)^{-2-\frac{L}{2}}}{\sqrt{4E_i E_j}}, \quad F_{kl}^{L'} = \frac{(1 + p_k^2/\Lambda^2)^{-2-\frac{L'}{2}}}{\sqrt{4E_k E_l}}, \quad (3)$$

where q_{ij} (p_k) and L (L') are the momentum and orbital angular momentum of i (k) in the ij (total) CM frame, respectively. The cutoff Λ_B , chosen to be independent of ij , are fitted to data, while $\Lambda = 1$ GeV is fixed.

The weak decays [Eq. (2)] are followed by coupled-channel rescatterings among the $\{D^{*0}\bar{D}^0\} - \{D^{*+}D^-\} - J/\psi\omega - J/\psi\rho - J/\psi\gamma - \psi'\gamma$ channels. We model the coupled-channel dynamics with separable s -wave potentials,

$$v_{\beta, \alpha}(q', q) = h_{\beta, \alpha} f_\beta^0(q', \Lambda_v) f_\alpha^0(q, \Lambda_v), \quad (4)$$

where α and β label the channels, $h_{\beta, \alpha}$ are coupling constants, and a cutoff Λ_v . Motivated by the OZI rule, we set $h_{\beta, \alpha} = 0$ if both α and β are in hidden-charm channels. We treat electromagnetic interactions to first order. The resulting $B^+ \rightarrow K^+ \alpha$ decay amplitude is

The $1/\sqrt{2}$ factor is due to projecting out the $C = +1$

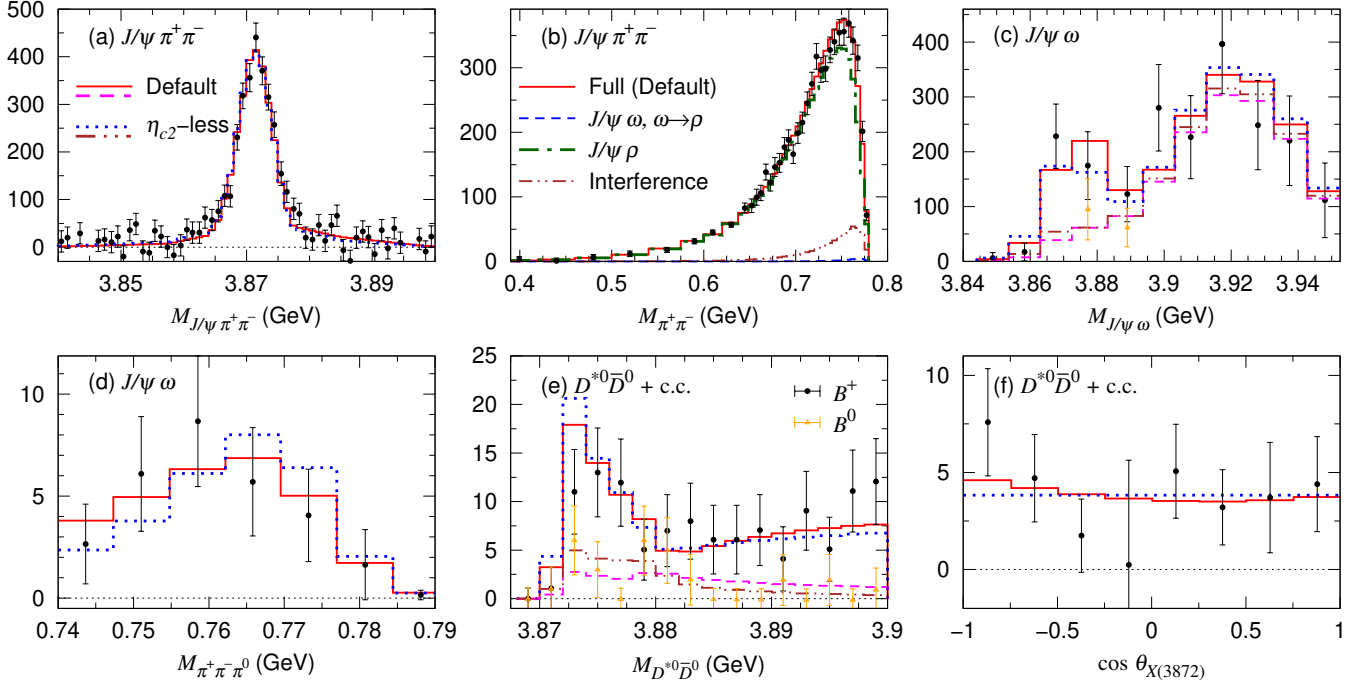


FIG. 2. (a)-(e) Invariant mass M_f and (f) helicity angle $\theta_{X(3872)}$ distributions for $B \rightarrow Kf$ where final states f are indicated in each panel; $B^+ \rightarrow K^+ f$ for (a)-(e), $B^0 \rightarrow K^0 f$ for (e), and an efficiency-weighted sum of $B^+ \rightarrow K^+ f$ and $B^0 \rightarrow K^0 f$ in (f). The units are events/bin. Histograms are obtained by smearing the corresponding theoretical curves with experimental resolutions and then averaging within each bin. In (c), the lower histograms and the data [orange triangle] are obtained by cutting off contributions from $M_{\pi^+\pi^-\pi^0} < 0.7695$ GeV. The legend in (a) applies to all panels except (b), which has its own legend. The data are from Ref. [60] in (a); [59] in (b); [38] in (c) and (d); [61] ($D^{*0} \rightarrow D^0 \pi^0$) in (e); [39] in (f). The uncorrected data points [orange triangle] in (c) are scaled to be comparable with the corrected data [black circles].

component of x . We introduced

$$[G^{-1}(p, E)]_{\beta\alpha} = \delta_{\beta\alpha} - h_{\beta,\alpha} \sigma_{\alpha}^{\Lambda_v \Lambda_v}(E), \quad (6)$$

and [58]

$$\sigma_{\alpha}^{\Lambda_1 \Lambda_2}(p, E) = \int dq q^2 \frac{M_{\alpha}(q)}{\sqrt{M_{\alpha}^2(q) + p^2}} \times \frac{f_{\alpha}^0(q, \Lambda_1) f_{\alpha}^0(q, \Lambda_2)}{E - \sqrt{M_{\alpha}^2(q) + p^2} + i \frac{\Gamma_{\alpha_1} + \Gamma_{\alpha_2}}{2}}, \quad (7)$$

with $M_{\alpha}(q) = E_{\alpha_1}(q) + E_{\alpha_2}(q)$; α_1 and α_2 are mesons forming α . The Green function $G_{\beta\alpha}$ of Eq. (6) violates the isospin due to the mass difference between $\{D^{*0} \bar{D}^0\}$ and $\{D^{*+} D^-\}$ channels. A corresponding $B^0 \rightarrow K^0 \alpha$ amplitude follows from Eq. (5) by replacing $B^+ \rightarrow B^0$ and $K^+ \rightarrow K^0$.

The $Y \rightarrow \gamma \alpha$ amplitude for Fig. 1(b) is obtained analogously. The η_{c2} and $\chi_{c0}(3915)$ excitation contributions to B and Y decays [Fig. 1(c)] are modeled with Breit-Wigner forms. We fit $m_{\eta_{c2}}$ to the data while taking a non-open-charm (nOC) partial width as $\Gamma_{\eta_{c2}}^{\text{nOC}} = 0.5$ MeV [47]. The $\chi_{c0}(3915)$ parameters are taken from Ref. [38]. For tree-level B^+ decay contributions [Fig. 1(d)], we use Eq. (2) and its $D\bar{D}^*$ counterpart; a tree-level Y decay amplitude is similar. LHCb

observed an $\omega - \rho$ mixing effect in the $M_{\pi^+\pi^-}$ distribution of $B^+ \rightarrow K^+ J/\psi \pi^+ \pi^-$ [59]. We add this mixing effect to the amplitudes discussed above. We also incorporate $\rho^0 \rightarrow \pi^+ \pi^-$ and $\omega \rightarrow \pi^+ \pi^- \pi^0$ decays when $\alpha = J/\psi \rho^0$ and $J/\psi \omega$, respectively. Amplitude expressions not shown here, together with formulas for differential decay widths, are provided in the Supplemental Material.

Results.— By fitting the experimental distributions⁴ in Figs. 2–3 and the ratios in Tables I–II, we obtain models A (default) and B that include all mechanisms of Fig. 1 (23 fit parameters). For comparison, we also construct an η_{c2} -less ($\not{\eta}_{c2}$) model by removing the mechanism in Fig. 1(c) (16 parameters). The parameter sets and experimental inputs (resolutions, efficiencies, and kinematic selections) into our calculations are summarized in the Supplemental Material.

Given that the datasets feature vastly different statistical uncertainties, we employ a weighted analysis to

⁴ For a decay chain $B \rightarrow Xc$ and $X \rightarrow ab$, a helicity angle [Fig. 2(f)] is given with momenta in the X -at-rest frame as $\cos \theta_X \equiv \frac{\mathbf{q}_a \cdot \mathbf{q}_B}{|\mathbf{q}_a| |\mathbf{q}_B|}$; $a = D^{*0}(\bar{D}^{*0})$ for Fig. 2(f) and 4(b), and $a = J/\psi$ or ψ' for Fig. 4(a).

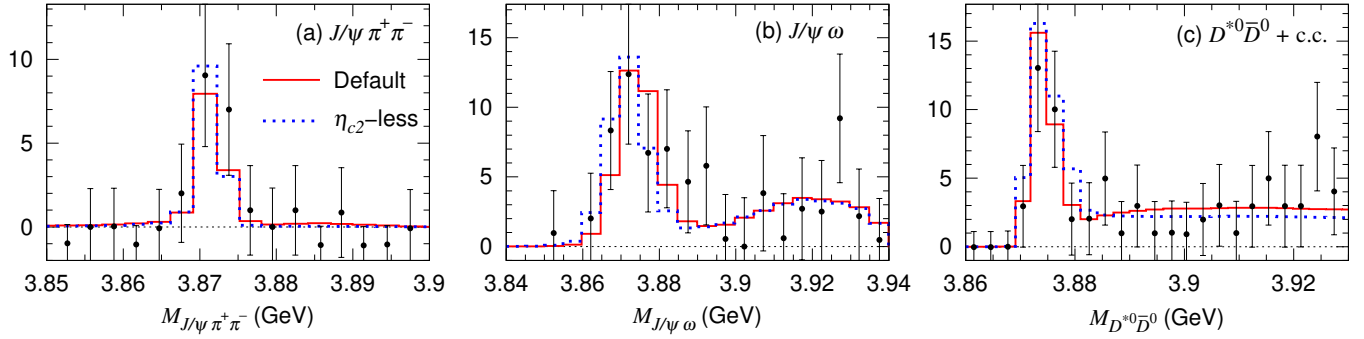


FIG. 3. Invariant mass (M_f) distributions for $e^+e^- \rightarrow \gamma f$ where final states f are indicated in each panel. The data are from Ref. [49] in (a); [48] in (b); [29] in (c).

obtain balanced fits. Consequently, we refrain from quoting formal parameter uncertainties, as they may not fully capture the underlying statistical and systematic effects. The extracted pole positions are $3871.4 - 0.022i$ MeV for $X(3872)$ and $3874. - 0.25i$ MeV for η_{c2} , slightly below and above the $D^{*0}\bar{D}^0$ threshold (3871.7 MeV), respectively. Within our model variants, these pole locations are stable.⁵

All three models give comparable fits to the lineshape data in Figs. 2–3. The differences between the default and η_{c2} models are within the experimental uncertainties. The slightly concave shape of the default model in Fig. 2(f) is due to η_{c2} . As demonstrated previously [59, 64], we also confirm in Fig. 2(b) that the $M_{\pi^+\pi^-}$ lineshape is formed by the main $X(3872) \rightarrow J/\psi\rho^0$ contribution ($J/\psi\rho'$ in the figure) and its interference with $X(3872) \rightarrow J/\psi\omega$ followed by the $\omega \rightarrow \rho$ mixing. In Fig. 2(e), the $M_{D^{*0}\bar{D}^0}$ lineshapes differ between B^+ and B^0 decays for $M_{D^{*0}\bar{D}^0} \gtrsim 3.88$ GeV. Our models explain this by the fact that the B^+ -decay amplitude features the color-favored tree mechanisms, while the B^0 -decay amplitude involves only color-suppressed ones.

The BABAR analysis [38] suggested that $X(3872)$ could be a 2^{-+} state by analyzing the $M_{\pi^+\pi^-\pi^0}$ distribution [Fig. 2(d)] where the ω tail governs the lineshape. Our default and η_{c2} models are consistent with the data after considering the resolution ($\sigma = 6$ MeV). Compared to our η_{c2} model, $1^+X(3872)$ in Ref. [38] produced a lineshape shifted to higher $M_{\pi^+\pi^-\pi^0}$. This is likely because $m_{X(3872)}$ of Ref. [38] is heavier at 3873.0 MeV, thereby including a larger ω contribution from the higher $M_{\pi^+\pi^-\pi^0}$ region. Thus, these data suggest that any state slightly above the $D^{*0}\bar{D}^0$ threshold cannot decay appreciably into s -wave $J/\psi\omega$. For $\eta_{c2} \rightarrow J/\psi\omega$ in a p wave, the centrifugal barrier suppresses the high-mass tail and prevents a shift to higher energies [38], as realized by the

default model in Fig. 2(d).

The ratios $\mathcal{R}_{B^0/B^+}(f) \equiv \frac{\Gamma[B^+ \rightarrow K^+ X(3872); X(3872) \rightarrow f]}{\Gamma[B^0 \rightarrow K^0 X(3872); X(3872) \rightarrow f]}$ are presented in Table I. This ratio should be independent of f , provided that the $X(3872)$ contribution is well isolated. The central values of the data are rather dependent on f , albeit the uncertainties are large. Our results from all models are consistent with the data, considering the large uncertainties. The η_{c2} model gives similar $\mathcal{R}_{B^0/B^+}(f)$ for different f , following the $X(3872)$ dominance. For the η_{c2} model, $\mathcal{R}_{B^0/B^+}(f) < 1$ can be understood from the facts [57] that: (i) Dominant color-favored B^+ (B^0) decays in Fig. 1(a) produce $\{D^{*0}\bar{D}^0\}$ ($\{D^{*+}D^-\}$); (ii) $X(3872)$ couples more strongly to $\{D^{*0}\bar{D}^0\}$ than to $\{D^{*+}D^-\}$. For the models A and B, $\mathcal{R}_{B^0/B^+}(f)$ are more dependent on f . This is because both $X(3872)$ and η_{c2} contribute and they have different partial decay widths for each f , and the $X(3872)$ production rate relative to η_{c2} 's is different between B^+ and B^0 decays.

The ratios \mathcal{R}_x [Eq. (1)] in Table II are a crucial quantity for determining the validity of the models. Our models A and B yield similar \mathcal{R}_x consistent with the data. However, the η_{c2} model significantly fails to reproduce the experimental $\mathcal{R}_{e^+e^-}(J/\psi\gamma, J/\psi\pi^+\pi^-)$, $\mathcal{R}_B^{\psi\gamma}$, and $\mathcal{R}_{e^+e^-}^{\psi\gamma}$. In particular, the η_{c2} model yields $\mathcal{R}_B^{\psi\gamma} \sim \mathcal{R}_{e^+e^-}^{\psi\gamma}$ since $X(3872) \rightarrow J/\psi\gamma, \psi'\gamma$ occur in the same way in B decays and e^+e^- annihilations. The models A and B give $\mathcal{R}_B^{\psi\gamma} \sim 6.4 \times \mathcal{R}_{e^+e^-}^{\psi\gamma}$ because $\psi'\gamma$ and $J/\psi\gamma$ are mainly from $X(3872)$ and η_{c2} decays, respectively, and

TABLE I. $\mathcal{R}_{B^0/B^+}(f)$ from A, B, and η_{c2} -less (η_{c2}) models. Data are from references indicated in the first row.

f	$J/\psi\pi^+\pi^-$ [65]	$J/\psi\omega$ [38]	$D^{*0}\bar{D}^0$ [61]	$J/\psi\gamma$ [27]	$\psi'\gamma$
A	0.56	0.83	1.1	1.0	0.43
B	0.55	0.82	1.1	1.0	0.42
η_{c2}	0.57	0.56	0.78	0.54	0.54
Exp.	0.50 ± 0.15	1.0 ± 0.6	$1.34^{+0.48}_{-0.42}$	$0.70^{+0.47}_{-0.40}$	–

⁵ See the Supplemental Material for the W_{c1} pole [62, 63].

TABLE II. $\mathcal{R}_x(f, J/\psi\pi^+\pi^-)$ [Eq. (1)]. (Left) $x = B$. (Right) $x = e^+e^-$. See Table I for other features.

f	$J/\psi\omega$ [38]	$D^{*0}\bar{D}^0$ [28, 61]	$J/\psi\gamma$ [27, 28]	$\mathcal{R}_B^{\psi\gamma}$ [30]	$J/\psi\omega$ [48]	$D^{*0}\bar{D}^0$ [29]	$J/\psi\gamma$ [29]	$\mathcal{R}_{e^+e^-}^{\psi\gamma}$ [29]
A	0.41	11.	0.20	1.6	2.0	14.	0.82	0.26
B	0.39	12.	0.19	1.6	1.9	13.	0.83	0.25
η_{c2}	0.72	12.	0.29	0.53	0.81	13.	0.22	0.53
Exp.	0.7 ± 0.3	$12.2^{+3.0}_{-2.6}$	0.22 ± 0.06	1.67 ± 0.25	1.6 ± 0.4	11.77 ± 3.09	0.79 ± 0.28	-0.04 ± 0.28

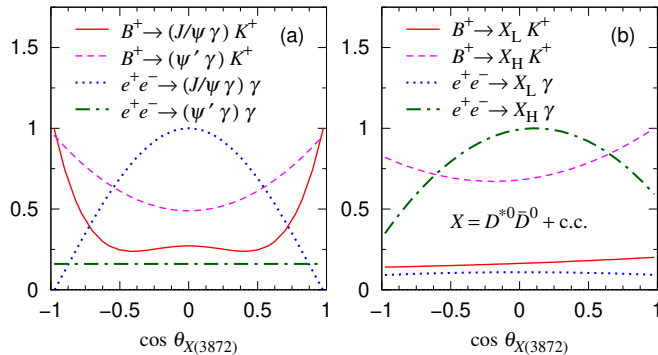


FIG. 4. Helicity angle distributions predicted by the default model. The unit is arbitrary; however, within each of panels (a) and (b), the model predicts the relative strengths of different final states from the same initial state. In (b), X_L and X_H contributions correspond to the integrated $M_{D^{*0}\bar{D}^0}$ regions. See the main text for details on the resolution smearing and integration procedures.

the production rate of η_{c2} relative to that of $X(3872)$ is larger in e^+e^- annihilations than in B decays. The comparisons in Table II indicate that the current data disfavor the η_{c2} model, and strongly support the hypothesis that $X(3872)$ is accompanied by a nearby state.

Recently, BESIII analyzed $e^+e^- \rightarrow \omega X(3872)$ data [66] and extracted the $X(3872)$ branching-fraction ratio $\mathcal{B}[X(3872) \rightarrow J/\psi\gamma]/\mathcal{B}[X(3872) \rightarrow J/\psi\pi^+\pi^-] = 0.38 \pm 0.20$, which is only marginally consistent with $\mathcal{R}_{e^+e^-}(J/\psi\gamma, J/\psi\pi^+\pi^-) = 0.79 \pm 0.28$. Even if they are confirmed to differ in the future, the two-state hypothesis can naturally accommodate the data since the cross-section ratio of $\sigma[e^+e^- \rightarrow \omega\eta_{c2}]/\sigma[e^+e^- \rightarrow \omega X(3872)]$ should be different from $\sigma[e^+e^- \rightarrow \gamma\eta_{c2}]/\sigma[e^+e^- \rightarrow \gamma X(3872)]$.

Having shown that the two-state hypothesis can account for the existing data, it is important to test it experimentally. We therefore provide helicity-angle⁴ distributions for several processes. Our predictions for $B^+ \rightarrow (\psi\gamma)K^+$ and $e^+e^- \rightarrow (\psi\gamma)\gamma$ ($\psi = J/\psi$ or ψ') are obtained by integrating over $3850 \leq M_{\psi\gamma} \leq 3890$ MeV and are shown in Fig. 4(a). Because this window is wide, we neglect resolution smearing in $M_{\psi\gamma}$. The angular dependence differs strongly between $J/\psi\gamma$ and $\psi'\gamma$ because the two channels are dominated by η_{c2} and $X(3872)$ de-

cays, respectively. If both final states were produced only through $X(3872)$ decays, the two distributions would instead follow the magenta dashed (green dash-dotted) curve for B^+ decay (e^+e^- annihilation).

We also predict helicity-angle distributions for the $D^{*0}\bar{D}^0 + \text{c.c.}$ final state [Fig. 4(b)]. Because both $X(3872)$ and η_{c2} contribute, we introduce simple kinematic selections to enhance one component at a time. We smear the $M_{D^{*0}\bar{D}^0}$ spectrum using the experimental resolution ($\sigma \sim 1$ MeV) of Ref. [29] and define X_L and X_H by integrating over $M_{D^{*0}\bar{D}^0} \leq 3872$ MeV and $3872 \leq M_{D^{*0}\bar{D}^0} \leq 3875$ MeV, respectively. With these definitions, X_L is dominated by $X(3872)$ while X_H is dominated by η_{c2} , leading to distinct angular dependences. If only a single $X(3872)$ state were present, both X_L and X_H would exhibit an approximately flat distribution.

Summary and outlook.— The radiative-decay ratios reported by LHCb and BESIII in the $X(3872)$ region are difficult to reconcile with a single isolated resonance. A minimal explanation is a nearby two-state structure: a shallow 1^{++} $D^{*0}\bar{D}^0$ bound state and a 2^{-+} charmonium candidate, η_{c2} , slightly above the $D^{*0}\bar{D}^0$ threshold. In this framework, we describe lineshapes and branching ratios across different production and decay channels, and we find that an explicit η_{c2} component is required to reproduce the radiative-ratio tension. Our helicity-angle predictions provide a direct experimental handle for testing the two-state scenario and searching for the missing η_{c2} .

The author acknowledges Pablo del Amo Sánchez, Christoph Hanhart, Atsushi Hosaka, Yanfeng Li, Chunhua Li, Zhiqing Liu, Kiyoshi Tanida, and Junhao Yin for useful discussions. This work is in part supported by Shandong Province Natural Science Foundation (Grant No. ZR2025MS56).

Supplemental Material

1. Formulas for amplitudes

We presented amplitude formulas in Eqs. (2) and (5). The formulas not shown in the main text are given below. The parameters in these amplitudes are determined by fitting data, as shown in Figs. 2 and 3 and Table I–II.

$$A_{Y \rightarrow \gamma \alpha}^{(b)} = (\boldsymbol{\epsilon}_\alpha \times \boldsymbol{\epsilon}_\gamma) \cdot \boldsymbol{\epsilon}_Y \sum_{\beta'} f_\alpha^0(q_\alpha, \Lambda_v) G_{\alpha, \beta'}(p_\gamma, E) \left(\begin{array}{c} \{D^{*0} \bar{D}^0\}, \{D^{*+} D^-\} \\ \sum_{\beta} h_{\beta', \beta} c_{\beta \gamma}^Y \sigma_{\beta}^{\Lambda_v, \Lambda_Y}(p_\gamma, E) \end{array} \right) F_{\gamma Y}^0(p_\gamma, \Lambda), \quad (9)$$

where $\boldsymbol{\epsilon}_\alpha$ is the total spin polarization of α . For example, $\boldsymbol{\epsilon}_\alpha = \boldsymbol{\epsilon}_{D^*}$ or $\boldsymbol{\epsilon}_{\bar{D}^*}$ for $\alpha = \{D^* \bar{D}\}$, and $\boldsymbol{\epsilon}_\alpha = (\boldsymbol{\epsilon}_x \times \boldsymbol{\epsilon}_{J/\psi})/\sqrt{2}$ for $\alpha = J/\psi x$ with $x = \omega, \rho^0, \gamma$.

For tree-level Y decay contributions [Fig. 1(d)], we use Eq. (8).

$$A_{B \rightarrow K \alpha}^{\eta_{c2}} = c_{\eta_{c2} K}^B c_\alpha^{\eta_{c2}} f_\alpha^1(q_\alpha, \Lambda_v) \frac{1}{2E_{\eta_{c2}}} \frac{\boldsymbol{\epsilon}_\alpha \cdot \mathbf{p}_K \mathbf{q}_\alpha \cdot \mathbf{p}_K - \frac{1}{3} \boldsymbol{\epsilon}_\alpha \cdot \mathbf{q}_\alpha p_K^2}{E - E_{\eta_{c2}} + i[\Gamma_{\eta_{c2}}^{D^* \bar{D}}(M_\alpha) + \Gamma_{\eta_{c2}}^{\text{nOC}}]/2} F_{KB}^2(p_K, \Lambda), \quad (10)$$

for $B \rightarrow K \alpha$ and $E = m_B - E_K$, and

$$A_{Y \rightarrow \gamma \alpha}^{\eta_{c2}} = c_{\eta_{c2} \gamma}^Y c_\alpha^{\eta_{c2}} f_\alpha^1(q_\alpha, \Lambda_v) \frac{1}{2E_{\eta_{c2}}} \frac{\boldsymbol{\epsilon}_Y \cdot [\mathbf{p}_\gamma \times (\frac{1}{2} \boldsymbol{\epsilon}_\alpha \cdot \boldsymbol{\epsilon}_\gamma \mathbf{q}_\alpha + \frac{1}{2} \mathbf{q}_\alpha \cdot \boldsymbol{\epsilon}_\gamma \boldsymbol{\epsilon}_\alpha - \frac{1}{3} \mathbf{q}_\alpha \cdot \boldsymbol{\epsilon}_\alpha \boldsymbol{\epsilon}_\gamma)]}{E - E_{\eta_{c2}} + i[\Gamma_{\eta_{c2}}^{D^* \bar{D}}(M_\alpha) + \Gamma_{\eta_{c2}}^{\text{nOC}}]/2} F_{\gamma Y}^1(p_\gamma, \Lambda), \quad (11)$$

for $Y \rightarrow \gamma \alpha$ and $E = m_Y - E_\gamma$; M_α is the invariant mass of α . Coupling constants for $B \rightarrow K \eta_{c2}$ and $Y \rightarrow \gamma \eta_{c2}$ are $c_{\eta_{c2} K}^B$ and $c_{\eta_{c2} \gamma}^Y$, respectively, and the $\eta_{c2} \rightarrow \alpha$ couplings are $c_\alpha^{\eta_{c2}}$. These coupling constants as well as $m_{\eta_{c2}}$ and $\Gamma_{\eta_{c2}}^{\text{nOC}}$ from non-open-charm (nOC) decay contributions are fitting parameters. Since $m_{\eta_{c2}}$ is close to the $D^* \bar{D}$ thresholds, we consider the energy dependence of the η_{c2} partial width for $\eta_{c2} \rightarrow D^* \bar{D}$ as

$$\Gamma_{\eta_{c2}}^{D^* \bar{D}}(M_\alpha) = 2\pi \frac{\left(c_{\{D^* \bar{D}\}}^{\eta_{c2}}\right)^2}{M_\alpha^2} \left[\frac{q_{D^{*0} \bar{D}^0}^3}{(1 + q_{D^{*0} \bar{D}^0}^2/\Lambda_v^2)^5} + \frac{q_{D^{*+} D^-}^3}{(1 + q_{D^{*+} D^-}^2/\Lambda_v^2)^5} \right], \quad (12)$$

The parameter values are given in Tables III–VI.

A. Mechanisms of Fig. 1(b) and 1(d)

The $Y(4230)$ decay vertices in Fig. 1(b) are

$$v_{\beta \gamma}^Y = c_{\beta \gamma}^Y f_\beta^0(q_\beta, \Lambda_Y) F_{Y \gamma}^0(p_\gamma, \Lambda) (\boldsymbol{\epsilon}_\beta \times \boldsymbol{\epsilon}_\gamma) \cdot \boldsymbol{\epsilon}_Y, \quad (8)$$

with $\beta = \{D^{*0} \bar{D}^0\}$ or $\{D^{*+} D^-\}$. The $Y \rightarrow \gamma \alpha$ amplitude is written, with $E = m_Y - E_\gamma$, by

B. Mechanisms of Fig. 1(c)

We use Breit–Wigner forms for the η_{c2} and $\chi_{c0}(3915)$ excitation amplitudes. The η_{c2} -excitation amplitude with $\alpha = \{D^{*0} \bar{D}^0\}$ or $J/\psi \omega$ is given by

where the denominators in the square bracket are from the square of the form factor $f_{D^* \bar{D}}^1(q_{D^* \bar{D}}, \Lambda_v)$; $M_\alpha = E_{D^*}(q_{D^* \bar{D}}) + E_{\bar{D}}(q_{D^* \bar{D}})$.

Similarly, the $\chi_{c0}(3915)$ excitation amplitude with $\alpha = J/\psi \omega$ is ($\chi'_{c0} \equiv \chi_{c0}(3915)$)

$$A_{B \rightarrow K \alpha}^{\chi'_{c0}} = \boldsymbol{\epsilon}_{J/\psi} \cdot \boldsymbol{\epsilon}_\omega c_{\chi'_{c0} K}^B c_\alpha^{\chi'_{c0}} f_\alpha^0(q_\alpha, \Lambda_v) \frac{1}{2E_{\chi'_{c0}}} \frac{1}{E - E_{\chi'_{c0}} + i \frac{\Gamma_{\chi'_{c0}}}{2}} F_{KB}^0(p_K, \Lambda), \quad (13)$$

for $B \rightarrow K \alpha$ and $E = m_B - E_K$, and

$$A_{Y \rightarrow \gamma \alpha}^{\chi'_{c0}} = \boldsymbol{\epsilon}_{J/\psi} \cdot \boldsymbol{\epsilon}_\omega \boldsymbol{\epsilon}_Y \cdot \boldsymbol{\epsilon}_\gamma c_{\chi'_{c0} \gamma}^Y c_\alpha^{\chi'_{c0}} f_\alpha^0(q_\alpha, \Lambda_v) \frac{1}{2E_{\chi'_{c0}}} \frac{1}{E - E_{\chi'_{c0}} + i \frac{\Gamma_{\chi'_{c0}}}{2}} F_{\gamma Y}^0(p_\gamma, \Lambda), \quad (14)$$

for $Y \rightarrow \gamma\alpha$ and $E = m_Y - E_\gamma$. The values of $m_{\chi'_{c0}}$ and $\Gamma_{\chi'_{c0}}$ are taken from Ref. [38].

C. $\rho^0 - \omega$ mixing

Let us define an amplitude $\bar{A}_{B \rightarrow K\alpha}$ by collecting the amplitudes discussed so far in Eqs. (5), (10), and (13) as

$$\bar{A}_{B \rightarrow K\alpha} = A_{B^+ \rightarrow K^+\alpha}^{(a)} + A_{B^+ \rightarrow K\alpha}^{\eta_{c2}} + A_{B^+ \rightarrow K\alpha}^{\chi'_{c0}}. \quad (15)$$

In addition, for $\alpha = J/\psi\rho^0$ or $J/\psi\omega$, we consider the $\rho^0 - \omega$ mixing. Thus, let us define an amplitude $A_{B \rightarrow K\alpha}$ by

$$A_{B \rightarrow KJ/\psi\rho^0} = \bar{A}_{B \rightarrow KJ/\psi\rho^0} - \frac{\epsilon_{\rho\omega}}{m_\omega^2 - \bar{m}_\omega^2 + i\bar{m}_\omega\bar{\Gamma}_\omega} \bar{A}_{B \rightarrow KJ/\psi\omega} \quad (16)$$

for $\alpha = J/\psi\rho^0$, and

$$A_{B \rightarrow KJ/\psi\omega} = \bar{A}_{B \rightarrow KJ/\psi\omega} - \frac{\epsilon_{\rho\omega}}{m_\rho^2 - \bar{m}_\rho^2 + i\bar{m}_\rho\bar{\Gamma}_\rho} \bar{A}_{B \rightarrow KJ/\psi\rho^0}, \quad (17)$$

for $\alpha = J/\psi\omega$, and

$$A_{B \rightarrow K\alpha} = \bar{A}_{B \rightarrow K\alpha}, \quad (18)$$

otherwise. We have introduced the $\rho^0 - \omega$ mixing parameter $\epsilon_{\rho\omega} = 3.35 \times 10^{-3} \text{ GeV}^2$ [64], and the nominal vector meson mass (\bar{m}_V) and width ($\bar{\Gamma}_V$) for $V = \rho^0$ and ω ; $\bar{m}_{\rho^0} = 775 \text{ MeV}$, $\bar{\Gamma}_{\rho^0} = 150 \text{ MeV}$, $\bar{m}_\omega = 783 \text{ MeV}$, and $\bar{\Gamma}_\omega = 8.49 \text{ MeV}$ [13]. The mass symbols m_ω in Eq. (16) and m_ρ in Eq. (17) are treated as variables, as will be seen below in Sec. 2 A.

Similarly, we include the $\rho^0 - \omega$ mixing for $Y \rightarrow \gamma\alpha$. We define an amplitude $\bar{A}_{Y \rightarrow \gamma\alpha}$ by summing the amplitudes in Eqs. (9), (11), and (14) as

$$\bar{A}_{Y \rightarrow \gamma\alpha} = A_{Y \rightarrow \gamma\alpha}^{(b)} + A_{Y \rightarrow \gamma\alpha}^{\eta_{c2}} + A_{Y \rightarrow \gamma\alpha}^{\chi'_{c0}}, \quad (19)$$

and the amplitudes $A_{Y \rightarrow \gamma\alpha}$, including the mixing effect, are obtained from Eqs. (16)–(18) by replacing $B \rightarrow Y$ and $K \rightarrow \gamma$.

D. Widths in Eq. (7)

For $\alpha = J/\psi\rho^0$, we use in Eq. (7) $\Gamma_{J/\psi} = 0$ and

$$\Gamma_{\rho^0}(M) = \bar{\Gamma}_{\rho^0} \frac{k^3}{\bar{k}^3} \left(\frac{\bar{m}_{\rho^0}}{M} \right)^2 \frac{(1 + \bar{k}^2/\Lambda_V^2)^5}{(1 + k^2/\Lambda_V^2)^5}, \quad (20)$$

with $\Lambda_V = 1 \text{ GeV}$, and the last factor is the ratio of squared form factors. The argument M denotes the invariant mass of $\pi^+\pi^-$ from ρ^0 decay, and k is the π^+ momentum in the ρ^0 -at-rest frame; \bar{k} is for $M = \bar{m}_{\rho^0}$. In Eq. (7), M is calculated using

$$M^2 = \left[\sqrt{E^2 - p^2} - E_{J/\psi}(q) \right]^2 - q^2. \quad (21)$$

For $\alpha = J/\psi\omega$, we again use Eq. (21) to determine M , and pass it to the total ω width of

$$\Gamma_\omega(M) = \Gamma_{\omega \rightarrow \pi^0\gamma}(M) + \Gamma_{\omega \rightarrow \pi^+\pi^-\pi^0}(M), \quad (22)$$

where

$$\Gamma_{\omega \rightarrow \pi^0\gamma}(M) = \bar{\Gamma}_\omega \mathcal{B}(\omega \rightarrow \pi^0\gamma) \left[\frac{\bar{m}_\omega(M^2 - m_{\pi^0}^2)}{M(\bar{m}_\omega^2 - m_{\pi^0}^2)} \right]^3, \quad (23)$$

with $\mathcal{B}(\omega \rightarrow \pi^0\gamma) = 0.0840$, and

$$\Gamma_{\omega \rightarrow \pi^+\pi^-\pi^0}(M) = c_1^\omega \left(\frac{M}{1 \text{ GeV}} + c_2^\omega \right)^{c_3^\omega}, \quad (24)$$

for $M \geq 2m_{\pi^\pm} + m_{\pi^0}$, and $\Gamma_{\omega \rightarrow \pi^+\pi^-\pi^0}(M) = 0$ otherwise; the parameters are $c_1^\omega = 1.061 \times 10^{-3} \text{ MeV}$, $c_2^\omega = 0.663$, and $c_3^\omega = 24.148$. To determine these parameters, we consider a $\omega \rightarrow \rho\pi$ ($\rho \rightarrow \pi\pi$) model including a Breit-Wigner ρ amplitude; all possible $\rho\pi$ charge states are included coherently. The $\omega \rightarrow \rho\pi$ coupling constant is fixed to reproduce $\Gamma_{\omega \rightarrow \pi^+\pi^-\pi^0}(\bar{m}_\omega) = \bar{\Gamma}_\omega \mathcal{B}(\omega \rightarrow \pi^+\pi^-\pi^0)$ with $\mathcal{B}(\omega \rightarrow \pi^+\pi^-\pi^0) = 0.892$. Then, the M dependence of $\Gamma_{\omega \rightarrow \pi^+\pi^-\pi^0}$ from this model is fitted with the parameterization of Eq. (24) in the region $M < 0.8 \text{ GeV}$.

For $\alpha = \{D^{*+}D^-\}$, M is determined using Eq. (21) where $E_{J/\psi}$ is replaced by E_{D^-} , and

$$\begin{aligned} \Gamma_{D^{*+}}(M) = & \Gamma_{D^{*+} \rightarrow D^0\pi^+}(M) \theta(M - m_{D^0} - m_{\pi^+}) \\ & + \Gamma_{D^{*+} \rightarrow D^+\pi^0}(M) \theta(M - m_{D^+} - m_{\pi^0}) \\ & + \Gamma_{D^{*+} \rightarrow D^+\gamma}(M - m_{D^+}), \end{aligned} \quad (25)$$

where $\theta(x)$ is the Heaviside step function, and

$$\Gamma_{D^{*+} \rightarrow D^0\pi^+}(M) = \frac{2}{3} 2\pi \frac{g_{D^*}^2 k_{\pi^+}^3}{M^2} \frac{1}{(1 + k_{\pi^+}^2/\Lambda_V^2)^5}, \quad (26)$$

$$\Gamma_{D^{*+} \rightarrow D^+\pi^0}(M) = \frac{1}{3} 2\pi \frac{g_{D^*}^2 k_{\pi^0}^3}{M^2} \frac{1}{(1 + k_{\pi^0}^2/\Lambda_V^2)^5}, \quad (27)$$

and $\Gamma_{D^{*+} \rightarrow D^+\gamma} = 1.33 \text{ keV}$; $g_{D^*} = 0.948$; $\Gamma_{D^{*+}}(m_{D^{*+}}) = 83.4 \text{ keV}$.

Similarly, for $\alpha = \{D^{*0}\bar{D}^0\}$, we use

$$\begin{aligned} \Gamma_{D^{*0}}(M) = & \Gamma_{D^{*0} \rightarrow D^0\pi^0}(M) \theta(M - m_{D^0} - m_{\pi^0}) \\ & + \Gamma_{D^{*0} \rightarrow D^+\pi^-}(M) \theta(M - m_{D^+} - m_{\pi^-}) \\ & + \Gamma_{D^{*0} \rightarrow D^0\gamma}(M - m_{D^0}), \end{aligned} \quad (28)$$

with

$$\Gamma_{D^{*0} \rightarrow D^0\pi^0}(M) = \frac{1}{3} 2\pi \frac{g_{D^*}^2 k_{\pi^0}^3}{M^2} \frac{1}{(1 + k_{\pi^0}^2/\Lambda_V^2)^5}, \quad (29)$$

$$\Gamma_{D^{*0} \rightarrow D^+\pi^-}(M) = \frac{2}{3} 2\pi \frac{g_{D^*}^2 k_{\pi^-}^3}{M^2} \frac{1}{(1 + k_{\pi^-}^2/\Lambda_V^2)^5}, \quad (30)$$

and $\Gamma_{D^{*0} \rightarrow D^0\gamma} = 19.4 \text{ keV}$; $\Gamma_{D^{*0}}(m_{D^{*0}}) = 55 \text{ keV}$.

TABLE III. B decay strength parameters and cutoff for models A, B, and η_{c2} , appearing in formulas indicated in the last column. Parameters not shown are related to those in the table by $c_{D^+D^*+K^+}^{B^+} = c_{D^*+D^-K^+}^{B^+}$, $c_{D^{*0}D^-K^0}^{B^0} = c_{D^*+D^-K^0}^{B^0}$, $c_{D^+D^*+K^0}^{B^0} = c_{D^0\bar{D}^*0K^+}^{B^+}$, $c_{D^{*0}\bar{D}^0K^0}^{B^0} = c_{D^*+D^-K^+}^{B^+}$, and $c_{D^0\bar{D}^*0K^0}^{B^0} = c_{D^+D^*+K^+}^{B^+}$.

	A	B	η_{c2}	Eq.
$c_{D^*0\bar{D}^0K^+}^{B^+} (\text{GeV}^{-1})$	-0.0178	-0.0554	0.0129	(2)
$c_{D^0\bar{D}^*0K^+}^{B^+} (\text{GeV}^{-1})$	$0.0450 + 0.0788i$	$0.0106 + 0.0708i$	$0.0564 - 0.0040i$	(2)
$c_{D^*+D^-K^+}^{B^+} (\text{GeV}^{-1})$	$-0.0206 + 0.0014i$	$-0.0129 - 0.0166i$	$-0.0042 - 0.0106i$	(2)
$c_{\eta_{c2}K}^B (\text{GeV}^{-1})$	-0.142	-0.135	-	(10)
$c_{\chi_{c0}K}^B (\text{GeV})$		1 (fixed)		(13)
$\Lambda_B (\text{GeV})$	0.703	0.759	1.496	(2)

TABLE IV. $Y(4230)$ decay strength parameters and cutoff.

	A	B	η_{c2}	Eq.
$c_{\{D^*0\bar{D}^0\}\gamma}^Y$	0.0193	0.0184	-0.0483	(8)
$c_{\{D^*+D^-\}\gamma}^Y$	-0.00374	-0.00361	-0.00964	(8)
$c_{\eta_{c2}\gamma}^Y$	-0.244	-0.222	-	(11)
$c_{\chi_{c0}\gamma}^Y (\text{GeV})$		1 (fixed)		(14)
$\Lambda_Y (\text{GeV})$	1.825	1.890	1.340	(8)

2. Formulas for differential decay width

The differential decay width (Dalitz plot distribution) for $B \rightarrow K f_1 f_2$ (f_1, f_2 form a final state f) is given by

$$\frac{d^2\Gamma_{B \rightarrow Kf}}{dM_{f_1 f_2}^2 dM_{K f_1}^2} = \frac{1}{(2\pi)^3} \frac{1}{32m_B^3} \frac{1}{2s_B + 1} \times \sum_{\text{spins}} |\mathcal{M}_{B \rightarrow Kf}|^2, \quad (31)$$

where the initial spin states are averaged, and all the final spin states are summed. The invariant amplitude $\mathcal{M}_{B \rightarrow Kf}$ is related to $A_{B \rightarrow Kf}$ by

$$\mathcal{M}_{B \rightarrow Kf} = -(2\pi)^3 \sqrt{2m_B} \sqrt{2E_K} \sqrt{2E_{f_1}} \sqrt{2E_{f_2}} \times A_{B \rightarrow Kf}, \quad (32)$$

where

$$A_{B \rightarrow Kf} = \frac{1}{\sqrt{2}} A_{B \rightarrow K\alpha} + v_{fK}^B \quad (33)$$

for $f = D^*0\bar{D}^0$ or $D^0\bar{D}^*0$, and $\alpha = \{D^*0\bar{D}^0\}$, and

$$A_{B \rightarrow Kf} = A_{B \rightarrow K\alpha}, \quad (34)$$

otherwise; we do not consider $f = D^*+D^-$ and D^+D^*- in this work. The amplitude $A_{B \rightarrow K\alpha}$ has been defined in Eqs. (15)–(18); v_{fK}^B is defined in Eq. (2); $A_{B^+ \rightarrow K^+ D^*0\bar{D}^0} \neq A_{B^+ \rightarrow K^+ D^0\bar{D}^*0}$ since $v_{D^*0\bar{D}^0K^+}^{B^+} \neq$

TABLE V. Coupling constants $h_{\beta,\alpha}$ and a cutoff Λ_v for $\{D^*0\bar{D}^0\} - \{D^*+D^-\} - J/\psi\omega - J/\psi\rho - J/\psi\gamma - \psi'\gamma$ coupled-channel scattering [Eq. (4)]. Parameters not shown are related to those shown in the table by $h_{\{D^*+D^-\},\{D^*+D^-\}} = h_{\{D^*0\bar{D}^0\},\{D^*0\bar{D}^0\}}$, $h_{\{D^*+D^-\},J/\psi\omega} = h_{\{D^*0\bar{D}^0\},J/\psi\omega}$, and $h_{\{D^*+D^-\},J/\psi\rho} = -h_{\{D^*0\bar{D}^0\},J/\psi\rho}$. The coupling parameters are also converted to the isospin basis, and are shown below the horizontal line. With an isospin state $|I, I_z\rangle$, a convention of $|D^{(*)+}\rangle = -|1/2, 1/2\rangle$ is used.

	A	B	η_{c2}
$h_{\{D^*0\bar{D}^0\},\{D^*0\bar{D}^0\}}$	-16.7	-17.1	-11.4
$h_{\{D^*0\bar{D}^0\},\{D^*+D^-\}}$	-8.52	-8.80	-8.59
$h_{\{D^*0\bar{D}^0\},J/\psi\omega}$	0.570	0.539	0.826
$h_{\{D^*0\bar{D}^0\},J/\psi\rho}$	2.28	2.21	1.74
$h_{\{D^*0\bar{D}^0\},J/\psi\gamma}$	-0.00	0.00	-0.146
$h_{\{D^*0\bar{D}^0\},\psi'\gamma}$	-0.255	-0.244	0.102
$h_{\{D^*+D^-\},J/\psi\gamma}$	-0.00	0.00	-0.146
$h_{\{D^*+D^-\},\psi'\gamma}$	-0.255	-0.244	0.102
$h_{\{D^*\bar{D}\}_{I=0},\{D^*\bar{D}\}_{I=0}}$	-25.2	-25.9	-20.0
$h_{\{D^*\bar{D}\}_{I=0},J/\psi\omega}$	-0.806	-0.762	-1.17
$h_{\{D^*\bar{D}\}_{I=0},J/\psi\gamma}$	0.00	0.00	0.206
$h_{\{D^*\bar{D}\}_{I=0},\psi'\gamma}$	0.361	0.345	-0.144
$h_{\{D^*\bar{D}\}_{I=1},\{D^*\bar{D}\}_{I=1}}$	-8.20	-8.28	-2.81
$h_{\{D^*\bar{D}\}_{I=1},J/\psi\rho}$	3.23	3.12	2.46
$h_{\{D^*\bar{D}\}_{I=1},J/\psi\gamma}$	-	-	-
$h_{\{D^*\bar{D}\}_{I=1},\psi'\gamma}$	-	-	-
$\Lambda_v (\text{GeV})$	0.818	0.800	1.012

$v_{D^0\bar{D}^*0K^+}^{B^+}$, while $A_{B^0 \rightarrow K^0 D^*0\bar{D}^0} = A_{B^0 \rightarrow K^0 D^0\bar{D}^*0}$ since $v_{D^*0\bar{D}^0K^0}^{B^0} = v_{D^0\bar{D}^*0K^0}^{B^0}$.

Regarding $e^+e^- \rightarrow \gamma f_1 f_2$, we first obtain $\mathcal{M}_{Y \rightarrow \gamma f}$ from Eqs. (32)–(34) by replacements $B \rightarrow Y$, $K \rightarrow \gamma$, and, then, $v_{f\gamma}^Y \rightarrow \frac{1}{\sqrt{2}} v_{\alpha\gamma}^Y$ in Eq. (33). $A_{Y \rightarrow \gamma\alpha}$ is defined in Eq. (19) and the following sentence; $v_{\alpha\gamma}^Y$ is defined in Eq. (8). Then we calculate differential cross sections for $e^+e^- \rightarrow \gamma f_1 f_2$ using Eq. (23) of Ref. [67] with

TABLE VI. η_{c2} and $\chi_{c0}(3915)$ mass, width, and decay strength parameters defined in Eqs. (10)–(14).

	A	B	η_{c2}
$m_{\eta_{c2}}$ (MeV)	3873.8	3874.6	–
$\Gamma_{\eta_{c2}}^{\text{OC}}$ (MeV)	0.5 (fixed)	0.5 (fixed)	–
$c_{\{D^{*0}\bar{D}^0\}}^{\eta_{c2}}$	0.198	–0.115	–
$c_{J/\psi\omega}^{\eta_{c2}}$	–0.111	–0.104	–
$c_{J/\psi\gamma}^{\eta_{c2}}$	–0.00617	0.00610	–
$c_{\psi'\gamma}^{\eta_{c2}}$	0.00002	–0.00000	–
$m_{\chi'_{c0}}$ (MeV)		3919.9 (fixed)	
$\Gamma_{\chi'_{c0}}$ (MeV)		31.0 (fixed)	
$c_{J/\psi\omega}^{\chi'_{c0}}$ (MeV)		1 (fixed)	

$\bar{\mathcal{M}}_{abc}^{\mu} = \mathcal{M}_{Y \rightarrow \gamma f} / [2M_Y(E - M_Y + i\frac{\Gamma_Y}{2})]$; the superfix μ is the polarization of $Y(4230)$.

For $B \rightarrow KD^{*0}\bar{D}^0$, we also calculate the helicity-angle ($\theta_{X(3872)}$) distribution; $\theta_{X(3872)}$ is the angle between the D^{*0} and B momenta in the $D^{*0}\bar{D}^0$ CM frame. We use the formula ($f = D^{*0}\bar{D}^0$ or $D^0\bar{D}^{*0}$):

$$\frac{d\Gamma_{B \rightarrow Kf}}{d \cos \theta_{X(3872)}} = \int \frac{d^2\Gamma_{B \rightarrow Kf}}{d \cos \theta_{X(3872)} dM_{f_1 f_2}} dM_{f_1 f_2} \quad (35)$$

with

$$\frac{d^2\Gamma_{B \rightarrow Kf}}{d \cos \theta_{X(3872)} dM_{f_1 f_2}} = \frac{d^2\Gamma_{B \rightarrow Kf}}{dM_{f_1 f_2}^2 dM_{K f_1}^2} \times 4m_B p_K q_{f_1}, \quad (36)$$

where p_K is the K momentum in the total CM frame and q_{f_1} is the f_1 momentum in the $f_1 f_2$ CM frame.

A. $\rho^0 \rightarrow \pi^+\pi^-$ and $\omega \rightarrow \pi^+\pi^-\pi^0$

For describing $B \rightarrow KJ/\psi\rho^0(\rho^0 \rightarrow \pi^+\pi^-)$ and $B \rightarrow KJ/\psi\omega(\omega \rightarrow \pi^+\pi^-\pi^0)$, $d\Gamma_{B \rightarrow KJ/\psi V} / dM_{J/\psi V}$ ($V = \rho^0, \omega$) of Eq. (31) is extended as follows:

$$\begin{aligned} \frac{d^2\Gamma_{B \rightarrow KJ/\psi\pi_V}}{dM_{J/\psi\pi_V} dM_{\pi_V}} &= \frac{1}{2\pi} \left. \frac{d\Gamma_{B \rightarrow KJ/\psi V}}{dM_{J/\psi V}} \right|_{m_V=M_{\pi_V}} \\ &\times \frac{[M_{\pi_V}/E_V]^2 \Gamma_{V \rightarrow \pi_V}(M_{\pi_V})}{|E - E_{J/\psi} - E_V + \frac{i}{2}\Gamma_V(M_{\pi_V})|^2}, \end{aligned} \quad (37)$$

where (V, π_V) is either $(\rho^0, \pi^+\pi^-)$ or $(\omega, \pi^+\pi^-\pi^0)$. $(d\Gamma_{B \rightarrow KJ/\psi V} / dM_{J/\psi V})|_{m_V=M_{\pi_V}}$ is calculated with Eq. (31) where the phase-space and the momenta involved depend on $m_V (= M_{\pi_V})$, and the V propagators in Eqs. (16) and (17) are also functions of m_V ; otherwise, $\mathcal{M}_{B \rightarrow Kf}$ in Eq. (31) does not depend on m_V . The nominal masses for ρ^0 and ω enter Eq. (37) through $E_V = \sqrt{\bar{m}_V^2 + \mathbf{p}_V^2}$. The total and partial V decay

widths are denoted by Γ_V and $\Gamma_{V \rightarrow \pi_V}$, respectively, and the formulas are given in Eqs. (20) and (22)–(24); $\Gamma_{\rho^0 \rightarrow \pi^+\pi^-} = \Gamma_{\rho^0}$.

For $e^+e^- \rightarrow \gamma J/\psi\rho^0(\rho^0 \rightarrow \pi^+\pi^-)$ and $e^+e^- \rightarrow \gamma J/\psi\omega(\omega \rightarrow \pi^+\pi^-\pi^0)$, we extend the cross-section formula in Eq. (23) of Ref. [67] in a manner similar to Eq. (37).

3. Experimental information

Experimental information considered in our calculations is summarized in Table VII. In the table, we refer to formulas below:

$$\begin{aligned} \sigma(M_{\pi^+\pi^-}) &= 2.39(1 - \exp(-M_{\pi^+\pi^-}/220.3)) \\ &\quad - 5.4 \exp(-M_{\pi^+\pi^-}/220.3), \end{aligned} \quad (38)$$

$$\begin{aligned} \epsilon(M_{\pi^+\pi^-}) &= 0.966 + 1.345 \times 10^{-3}(M_{\pi^+\pi^-} - 700) \\ &\quad + 1.607 \times 10^{-6}(M_{\pi^+\pi^-} - 700)^2, \end{aligned} \quad (39)$$

with $\sigma(M_{\pi^+\pi^-})$ and $M_{\pi^+\pi^-}$ being in MeV.

4. W_{c1} pole

Our coupled-channel models of Eq. (4) with their parameters in Table V have a virtual pole near the $D^{*+}D^-$ threshold (unphysical sheet). The pole position is $3882.8 + 1.5i$ MeV for model A, $3882.7 + 1.5i$ MeV for model B, and $3882.3 + 3.1i$ for η_{c2} model. The existence of this pole, called W_{c1} , was pointed out in Ref. [62] and further studied in Ref. [63]. Our results are similar to the one in Ref. [63]. The W_{c1} pole would enhance the $D^{*+}D^-$ threshold cusp, which may be seen, for example, in $B^0 \rightarrow K^0(D^{*0}\bar{D}^0 + \text{c.c.})$ [Fig. 2(e)].

TABLE VII. Experimental information considered in our calculations. Observables are partial widths Γ_p and cross sections σ_p for processes p . We do not apply cuts to kinematical variables other than those shown in 'kinematical regions'. Resolutions are given by the standard deviations (σ) of the gaussian distribution. Experimental information in the curly brackets are chosen by ourselves, while the others are taken from references in the column 'Ref.'. Hyphens indicate that resolution and/or efficiency are not considered. The calculated observables are shown in tables and figures indicated in the last column.

process (p)	observable	kinematical regions (MeV)	σ (MeV)	efficiency	Ref.
$B^+ \rightarrow K^+ J/\psi \pi^+ \pi^-$	Γ_p	$\{3850 \leq M_{J/\psi \pi^+ \pi^-} \leq 3890\}$	–	–	– Tables I,II
	$d\Gamma_p/dM_{J/\psi \pi^+ \pi^-}$	–	2.6	–	[60] Fig. 2(a)
	$d\Gamma_p/dM_{\pi^+ \pi^-}$	$\{3869 \leq M_{J/\psi \pi^+ \pi^-} \leq 3873\}$	Eq. (38)	Eq. (39)	[59] Fig. 2(b)
$B^0 \rightarrow K^0 J/\psi \pi^+ \pi^-$	Γ_p	$\{3850 \leq M_{J/\psi \pi^+ \pi^-} \leq 3890\}$	–	–	– Table I
$B^+ \rightarrow K^+ J/\psi \omega$	Γ_p^a	$\left\{ \begin{array}{l} 740 \leq M_{\pi^+ \pi^- \pi^0} \leq 796.5 \\ \{3850 \leq M_{J/\psi \omega} \leq 3890\} \end{array} \right.$	–	–	[38] Tables I,II
	$d\Gamma_p/dM_{J/\psi \omega}$	$740 \leq M_{\pi^+ \pi^- \pi^0} \leq 796.5$	6.7	–	[38] Fig. 2(c)
	$d\Gamma_p/dM_{J/\psi \omega}$	$769.5 \leq M_{\pi^+ \pi^- \pi^0} \leq 796.5$	6.7	–	[38] Fig. 2(c)
	$d\Gamma_p/dM_{\pi^+ \pi^- \pi^0}$	$3862.5 \leq M_{J/\psi \pi^+ \pi^- \pi^0} \leq 3882.5$	$\{6\}^b$	–	[38] Fig. 2(d)
$B^0 \rightarrow K^0 J/\psi \omega$	Γ_p^a	$\left\{ \begin{array}{l} 740 \leq M_{\pi^+ \pi^- \pi^0} \leq 805.5 \\ \{3850 \leq M_{J/\psi \omega} \leq 3890\} \end{array} \right.$	–	–	[38] Table I
$B^{+(0)} \rightarrow K^{+(0)} D^{*0} \bar{D}^0 + K^{+(0)} D^0 \bar{D}^{*0}$	Γ_p^c	$\{M_{D^{*0} \bar{D}^0} \leq 3900\}$	–	–	– Tables I,II
	$d\Gamma_p/dM_{D^{*0} \bar{D}^0}$	–	See Ref.	See Ref.	[61, 68] Fig. 2(e)
	$d\Gamma_p/d \cos \theta_{X(3872)}^d$	$\{M_{D^{*0} \bar{D}^0} \leq 3880\}$	–	$\left\{ \begin{array}{l} 4.3 \times 10^{-4} (B^+) \\ 0.7 \times 10^{-4} (B^0) \end{array} \right.$	[39] Fig. 2(f)
	$d\Gamma_p^{X^L}/d \cos \theta_{X(3872)}$	$\{M_{D^{*0} \bar{D}^0} \leq 3872\}$	~ 1	–	[29] Fig. 4(b)
	$d\Gamma_p^{X^H}/d \cos \theta_{X(3872)}$	$\{3872 \leq M_{D^{*0} \bar{D}^0} \leq 3875\}$	~ 1	–	[29] Fig. 4(b)
$B^{+(0)} \rightarrow K^{+(0)} J/\psi \gamma$	Γ_p	$\{3850 \leq M_{J/\psi \gamma} \leq 3890\}$	–	–	– Tables I,II
	$d\Gamma_p/d \cos \theta_{X(3872)}$	$\{3850 \leq M_{J/\psi \gamma} \leq 3890\}$	–	–	– Fig. 4(a)
$B^{+(0)} \rightarrow K^{+(0)} \psi' \gamma$	Γ_p	$\{3850 \leq M_{\psi' \gamma} \leq 3890\}$	–	–	– Tables I,II
	$d\Gamma_p/d \cos \theta_{X(3872)}$	$\{3850 \leq M_{\psi' \gamma} \leq 3890\}$	–	–	– Fig. 4(a)
$e^+ e^- \rightarrow \gamma J/\psi \pi^+ \pi^-$	σ_p	$\{3850 \leq M_{J/\psi \pi^+ \pi^-} \leq 3890\}$	–	–	– Table II
	$d\sigma_p/dM_{J/\psi \pi^+ \pi^-}$	–	1.14	–	[49] Fig. 3(a)
$e^+ e^- \rightarrow \gamma J/\psi \omega$	σ_p^a	$\left\{ \begin{array}{l} 720 \leq M_{\pi^+ \pi^- \pi^0} \leq 810 \\ \{3850 \leq M_{J/\psi \omega} \leq 3890\} \end{array} \right.$	–	–	[48] Table II
	$d\sigma_p/dM_{J/\psi \omega}$	$720 \leq M_{\pi^+ \pi^- \pi^0} \leq 810$	4.3	–	[48] Fig. 3(b)
$e^+ e^- \rightarrow \gamma (D^{*0} \bar{D}^0 + \text{c.c.})$	σ_p^e	$\{M_{D^{*0} \bar{D}^0} \leq 3900\}$	–	–	– Table II
	$d\sigma_p/dM_{D^{*0} \bar{D}^0}$	–	~ 1	–	[29] Fig. 3(c)
	$d\sigma_p^{X^L}/d \cos \theta_{X(3872)}$	$\{M_{D^{*0} \bar{D}^0} \leq 3872\}$	~ 1	–	[29] Fig. 4(b)
	$d\sigma_p^{X^H}/d \cos \theta_{X(3872)}$	$\{3872 \leq M_{D^{*0} \bar{D}^0} \leq 3875\}$	~ 1	–	[29] Fig. 4(b)
$e^+ e^- \rightarrow \gamma J/\psi \gamma$	σ_p	$\{3850 \leq M_{J/\psi \gamma} \leq 3890\}$	–	–	– Table II
	$d\sigma_p/d \cos \theta_{X(3872)}$	$\{3850 \leq M_{J/\psi \gamma} \leq 3890\}$	–	–	– Fig. 4(a)
$e^+ e^- \rightarrow \gamma \psi' \gamma$	σ_p	$\{3850 \leq M_{\psi' \gamma} \leq 3890\}$	–	–	– Table II
	$d\sigma_p/d \cos \theta_{X(3872)}$	$\{3850 \leq M_{\psi' \gamma} \leq 3890\}$	–	–	– Fig. 4(a)

^a $\chi_{c0}(3915)$ contribution is not included. $\mathcal{B}(\omega \rightarrow \pi^+ \pi^- \pi^0) = 89.2\%$ [13] is used to convert $\pi^+ \pi^- \pi^0$ to ω final state.

^b This resolution is obtained from fitting the η peak in Fig. 1 of Ref. [38].

^c Γ_p from our full calculations are multiplied by 42% (B^+) and 58% (B^0) to compare with data; Fig. 4(right) of Ref. [61] shows their analysis result where the $X(3872)$ contributions are $\sim 42\%$ (B^+) and $\sim 58\%$ (B^0) of the full contribution for $M_{D^{*0} \bar{D}^0} \leq 3900$ MeV.

^d B^+ and B^0 decay results are multiplied by their efficiencies, respectively, and then summed.

^e σ_p from our full calculation is multiplied by 59% to compare with data; Fig. 2(e) of Ref. [29] shows their analysis result where the $X(3872)$ contribution is $\sim 59\%$ of the full contribution for $M_{D^{*0} \bar{D}^0} \leq 3900$ MeV.

* satoshi@sdu.edu.cn

- [1] S.-K. Choi et al. (Belle Collaboration), Observation of a Narrow Charmoniumlike State in Exclusive $B^\pm \rightarrow K^\pm \pi^+ \pi^- J/\psi$ Decays, *Phys. Rev. Lett.* **91**, 262001 (2003).
- [2] H.-X. Chen, W. Chen, X. Liu, and S.-L. Zhu, The hidden-charm pentaquark and tetraquark states, *Phys. Rep.* **639**, 1 (2016).
- [3] A. Hosaka, T. Iijima, K. Miyabayashi, Y. Sakai, and S. Yasui, Exotic hadrons with heavy flavors: X , Y , Z , and related states, *PTEP* **2016**, 062C01 (2016).
- [4] R.F. Lebed, R.E. Mitchell, and E.S. Swanson, Heavy-Quark QCD Exotica, *Prog. Part. Nucl. Phys.* **93**, 143 (2017).
- [5] A. Esposito, A. Pilloni, and A.D. Polosa, Multiquark Resonances, *Phys. Rept.* **668**, 1 (2017).
- [6] A. Ali, J.S. Lange, and S. Stone, Exotics: Heavy Pentaquarks and Tetraquarks, *Prog. Part. Nucl. Phys.* **97**, 123 (2017).
- [7] F.-K. Guo, C. Hanhart, U.-G. Meißner, Q. Wang, Q. Zhao, and B.-S. Zou, Hadronic molecules, *Rev. Mod. Phys.* **90**, 015004 (2018).
- [8] S.L. Olsen, T. Skwarnicki, and D. Zieminska, Nonstandard heavy mesons and baryons: Experimental evidence, *Rev. Mod. Phys.* **90**, 015003 (2018).
- [9] N. Brambilla, S. Eidelman, C. Hanhart, A. Nefediev, C.-P. Shen, C.E. Thomas, A. Vairo, and C.-Z. Yuan, The XYZ states: Experimental and theoretical status and perspectives, *Phys. Rept.* **873**, 1 (2020).
- [10] A. Esposito, A. Glioti, D. Germani, and A.D. Polosa, A short review on the compositeness of the $X(3872)$, *Riv. Nuovo Cim.* **48**, 95 (2025).
- [11] S. Godfrey and N. Isgur, Mesons in a Relativized Quark Model with Chromodynamics, *Phys. Rev. D* **32**, 189 (1985).
- [12] T. Barnes and S. Godfrey, Charmonium options for the $X(3872)$, *Phys. Rev. D* **69**, 054008 (2004).
- [13] S. Navas et al. (Particle Data Group), Review of Particle Physics, *Phys. Rev. D* **110**, 030001 (2024).
- [14] E.S. Swanson, Short range structure in the $X(3872)$, *Phys. Lett. B* **588**, 189 (2004).
- [15] E. Braaten, M. Kusunoki, and S. Nussinov, Production of the $X(3872)$ in B -Meson Decay by the Coalescence of Charm Mesons, *Phys. Rev. Lett.* **93**, 162001 (2004).
- [16] I.-W. Lee, A. Faessler, T. Gutsche, and V.E. Lyubovitskij, $X(3872)$ as a molecular DD^* state in a potential model, *Phys. Rev. D* **80**, 094005 (2009).
- [17] F.-K. Guo, C. Hanhart, U.-G. Meißner, Q. Wang, and Q. Zhao, Production of the $X(3872)$ in charmonia radiative decays, *Phys. Lett. B* **725**, 127 (2013).
- [18] Yu.S. Kalashnikova, Coupled-channel model for charmonium levels and an option for $X(3872)$, *Phys. Rev. D* **72**, 034010 (2005).
- [19] M. Suzuki, The $X(3872)$ boson: Molecule or charmonium, *Phys. Rev. D* **72**, 114013 (2005).
- [20] C. Bignamini, B. Grinstein, F. Piccinini, A.D. Polosa, and C. Sabelli, Is the $X(3872)$ Production Cross Section at $\sqrt{s} = 1.96$ TeV Compatible with a Hadron Molecule Interpretation? *Phys. Rev. Lett.* **103**, 162001 (2009).
- [21] CMS Collaboration, Measurement of the $X(3872)$ production cross section via decays to $J/\psi \pi^+ \pi^-$ in pp collisions at $\sqrt{s} = 7$ TeV, *J. High Energ. Phys.* **2013**, 154 (2013).
- [22] C. Meng, H. Han, K.-T. Chao, $X(3872)$ and its production at hadron colliders, *Phys. Rev. D* **96**, 074014 (2017).
- [23] R. Aaij et al. (LHCb Collaboration), Observation of multiplicity dependent prompt $\chi_{c1}(3872)$ and $\psi(2S)$ production in pp collisions, *Phys. Rev. Lett.* **126**, 092001 (2021).
- [24] A. Esposito, E.G. Ferreira, A. Pilloni, A.D. Polosa, and C.A. Salgado, The nature of $X(3872)$ from high-multiplicity pp collisions, *Eur. Phys. J. C* **81**, 669 (2021).
- [25] S. Prelovsek and L. Leskovec, Evidence for $X(3872)$ from DD^* Scattering on the Lattice, *Phys. Rev. Lett.* **111**, 192001 (2013).
- [26] M. Padmanath, C.B. Lang, and S. Prelovsek, $X(3872)$ and $Y(4140)$ using diquark-antidiquark operators with lattice QCD, *Phys. Rev. D* **92**, 034501 (2015).
- [27] V. Bhardwaj et al. (Belle Collaboration), Observation of $X(3872) \rightarrow J/\psi \gamma$ and Search for $X(3872) \rightarrow \psi' \gamma$ in B Decays, *Phys. Rev. Lett.* **107**, 091803 (2011).
- [28] R. Aaij et al. (LHCb Collaboration), Study of the $\psi_2(3823)$ and $\chi_{c1}(3872)$ states in $B^+ \rightarrow (J/\psi \pi^+ \pi^-) K^+$ decays, *J. High Energ. Phys.* **2020**, 123 (2020).
- [29] M. Ablikim et al. (BESIII Collaboration), Study of Open-Charm Decays and Radiative Transitions of the $X(3872)$, *Phys. Rev. Lett.* **124**, 242001 (2020).
- [30] R. Aaij et al. (LHCb Collaboration), Probing the nature of the $\chi_{c1}(3872)$ state using radiative decays, *J. High Energ. Phys.* **2024**, 121 (2024).
- [31] R. Aaij et al. (LHCb Collaboration), Determination of the $X(3872)$ meson quantum numbers, *Phys. Rev. Lett.* **110**, 222001 (2013).
- [32] C. Hidalgo-Duque, J. Nieves, and M.P. Valderrama, Light flavor and heavy quark spin symmetry in heavy meson molecules, *Phys. Rev. D* **87**, 076006 (2013).
- [33] F.-K. Guo, C. Hidalgo-Duque, J. Nieves, A. Ozpineci, and M.P. Valderrama, Detecting the long-distance structure of the $X(3872)$, *Eur. Phys. J. C* **74**, 2885 (2014).
- [34] P.G. Ortega, D.R. Entem and F. Fernandez, Molecular structures in charmonium spectrum: The XYZ puzzle, *J. Phys. G* **40**, 065107 (2013).
- [35] F.-K. Guo, C. Hanhart, Yu.S. Kalashnikova, U.-G. Meißner, and A.V. Nefediev, What can radiative decays of the $X(3872)$ teach us about its nature?, *Phys. Lett. B* **742**, 394 (2015).
- [36] E. Cincioglu, J. Nieves, A. Ozpineci, and A.U. Yilmazer, Quarkonium Contribution to Meson Molecules, *Eur. Phys. J. C* **76**, 576 (2016).
- [37] S. Takeuchi, M. Takizawa, and K. Shimizu, Radiative Decays of the $X(3872)$ in the Charmonium-Molecule Hybrid Picture, *JPS Conf.Proc.* **17**, 112001 (2017).
- [38] P. del Amo Sanchez et al. (BABAR Collaboration), Evidence for the decay $X(3872) \rightarrow J/\psi \omega$, *Phys. Rev. D* **82**, 011101(R) (2010).
- [39] B. Aubert et al. (BABAR Collaboration), Study of resonances in exclusive B decays to $\bar{D}^{(*)} D^{(*)} K$, *Phys. Rev. D* **77**, 011102(R) (2008).
- [40] L.P. Fulcher, Perturbative QCD, a universal QCD scale, long-range spin-orbit potential, and the properties of heavy quarkonia, *Phys. Rev. D* **44**, 2079 (1991).
- [41] J.J. Dudek, R.G. Edwards, N. Mathur, and D.G. Richards, Charmonium excited state spectrum in lattice QCD, *Phys. Rev. D* **77**, 034501 (2008).
- [42] Y.-B. Yang, Y. Chen, L.-C. Gui, C. Liu, Y.-B. Liu, Z. Liu,

- J.-P. Ma, and J.-B. Zhang (CLQCD Collaboration), Lattice study on η_{c2} and $X(3872)$, Phys. Rev. D **87**, 014501 (2013).
- [43] K. Chilikin et al. (Belle collaboration), First search for the $\eta_{c2}(1D)$ in B decays at Belle, J. High Energ. Phys. **2020**, 34 (2020).
- [44] S. Jia et al. (Belle Collaboration), Search for the $\eta_{c2}(1D)$ in $e^+e^- \rightarrow \gamma\eta_{c2}(1D)$ at \sqrt{s} near 10.6 GeV at Belle, Phys. Rev. D **104**, 012012 (2021).
- [45] K.J. Sebastian and X. G. Zhang, Radiative transitions of the D states of charmonium in potential models, Phys. Rev. D **55**, 225 (1997).
- [46] Y. Jia, W.-L. Sang, and J. Xu, Is the $J^P = 2^-$ assignment for the $X(3872)$ compatible with the radiative transition data?, arXiv:1007.4541.
- [47] X.-Y. Du, S.-Y. Pei, W. Li, M. Jia, Q. Li, T. Wang, B. Wang, and G.-L. Wang, $\eta_{c2}(1D)$ and its electromagnetic decays, Phys. Rev. D **110**, 113009 (2024).
- [48] M. Ablikim et al. (BESIII Collaboration), Study of $e^+e^- \rightarrow \gamma\omega J/\psi$ and Observation of $X(3872) \rightarrow \omega J/\psi$, Phys. Rev. Lett. **122**, 232002 (2019).
- [49] M. Ablikim et al. (BESIII Collaboration), Observation of $e^+e^- \rightarrow \gamma X(3872)$ at BESIII, Phys. Rev. Lett. **112**, 092001 (2014).
- [50] T.J. Burns, F. Piccinini, A.D. Polosa, and C. Sabelli The 2^{-+} assignment for the $X(3872)$, Phys. Rev. D **82**, 074003 (2010).
- [51] Yu. S. Kalashnikova and A. V. Nefediev, $X(3872)$ as 1D_2 charmonium state, Phys. Rev. D **82**, 097502 (2010).
- [52] H.-W. Ke and X.-Q. Li, What do the radiative decays of $X(3872)$ tell us, Phys. Rev. D **84**, 114026 (2011).
- [53] J.-Z. Wang, Z.-Y. Lin, Y.-K. Chen, L. Meng, and S.-L. Zhu, Uncovering the mystery of $X(3872)$ with the coupled-channel dynamics, Phys. Rev. D **111**, L111502 (2025).
- [54] P.-P. Shi, M. Albaladejo, M.-L. Du, F.-K. Guo, and J. Nieves, P -wave charmonium contribution to hidden-charm states from a reanalysis of lattice QCD data, Phys. Rev. D **111**, 074043 (2025).
- [55] J.P. Lees et al. (BaBar Collaboration), Study of $X(3915) \rightarrow J/\psi\omega$ in two-photon collisions, Phys. Rev. D **86**, 072002 (2012).
- [56] Z.-Y. Zhou, Z. Xiao, and H.-Q. Zhou, Could the $X(3915)$ and the $X(3930)$ Be the Same Tensor State? Phys. Rev. Lett. **115**, 022001 (2015).
- [57] H.-N. Wang, L.-S. Geng, Q. Wang, and J.-J. Xie, Molecular Nature of $X(3872)$ in $B^0 \rightarrow K^0 X(3872)$ and $B^+ \rightarrow K^+ X(3872)$ Decays, Chinese Phys. Lett. **40**, 021301 (2023).
- [58] H. Kamano, B. Juliá-Díaz, T.-S. H. Lee, A. Matsuyama, and T. Sato, Dynamical coupled-channels study of $\pi N \rightarrow \pi\pi N$ reactions, Phys. Rev. C **79**, 025206 (2009).
- [59] R. Aaij et al. (LHCb Collaboration), Observation of sizeable ω contribution to $\chi_{c1}(3872) \rightarrow \pi^+\pi^- J/\psi$ decays, Phys. Rev. D **108**, L011103 (2023).
- [60] R. Aaij et al. (LHCb Collaboration), Study of the line-shape of the $\chi_{c1}(3872)$ state, Phys. Rev. D **102**, 092005 (2020).
- [61] H. Hirata et al. (Belle Collaboration), Study of the line-shape of $X(3872)$ using B decays to $D^0\bar{D}^{*0}K$, Phys. Rev. D **107**, 112011 (2023).
- [62] Z.-H. Zhang, T. Ji, X.-K. Dong, F.-K. Guo, C. Hanhart, U.-G. Meißner, and A. Rusetsky, Predicting isovector charmonium-like states from $X(3872)$ properties, JHEP **08**, 130 (2024).
- [63] T. Ji, X.-K. Dong, F.-K. Guo, C. Hanhart, and U.-G. Meißner, Precise determination of the properties of $X(3872)$ and of its isovector partner W_{c1} , arXiv:2502.04458 [hep-ph].
- [64] J.M. Dias, T. Ji, X.-K. Dong, F.-K. Guo, C. Hanhart, U.-G. Meißner, Y. Zhang, and Z.-H. Zhang, Dispersive analysis of the isospin breaking in the $X(3872) \rightarrow J/\psi\pi^+\pi^-$ and $X(3872) \rightarrow J/\psi\pi^+\pi^0\pi^-$ decays, Phys. Rev. D **111**, 014031 (2025).
- [65] S.-K. Choi et al. (Belle Collaboration), Bounds on the width, mass difference and other properties of $X(3872) \rightarrow \pi^+\pi^- J/\psi$ decays, Phys. Rev. D **84**, 052004 (2011).
- [66] M. Ablikim et al. (BESIII Collaboration), Study of $e^+e^- \rightarrow \omega X(3872)$ and $\gamma X(3872)$ from 4.66 to 4.95 GeV, Phys. Rev. D **110**, 012006 (2024).
- [67] S.X. Nakamura, X.-H. Li, H.-P. Peng, Z.-T. Sun, and X.-R. Zhou, Global coupled-channel analysis of $e^+e^- \rightarrow c\bar{c}$ processes in $\sqrt{s} = 3.75$ to 4.7 GeV, Phys. Rev. D **112**, 054027 (2025).
- [68] H. Hirata, Study of the $X(3872)$ Invariant Mass Distribution Using the $B \rightarrow (X(3872) \rightarrow D^0\bar{D}^{*0})K$ Decay at the Belle Experiment, PhD thesis (Nagoya University); <http://hdl.handle.net/2237/0002005652>